Nonlinear wave dynamics in Faraday instabilities

Peilong Chen
Department of Physics and Center for Complex Systems, National Central University, Chungli 320, Taiwan
(Received 20 June 2001; published 15 February 2002)

Nonlinear wave dynamics in parametrically driven surface waves are studied in numerical simulations of the two-dimensional Navier-Stokes equation, with an emphasis on the evolution and interaction between different wave number modes. The dynamics are found to be closely correlated with the single-mode nonlinear saturated wave amplitudes. Modulating behavior of primary wave modes in a particular parameter range and in time scales much longer than the underlining wave periods is observed.

DOI: 10.1103/PhysRevE.65.036308 PACS number(s): 47.20.Ky, 47.35.+i, 47.54.+r

I. INTRODUCTION

In this paper wave dynamics of parametrically excited surface waves (also called Faraday waves) are studied in numerical simulations of the two-dimensional Navier–Stokes equation. Faraday waves are excited (usually subharmonically) when a fluid layer with a free surface is subjected to periodic vertical acceleration [1]. In such a system, there is a minimum accelerating amplitude at which waves appear at a critical wave number. The characteristics of rich phenomenology, easily adjustable spatial and temporal scales, moderate demands on experimental setup, and well established underlying microscopic equations [2] have made Faraday waves an ideal system in which to study pattern formation in driving-dissipative systems [3]. Here the microscopic equations refer not to the atomic picture but rather to the generally accepted continuum description of fluids. In some recent experiments using non-Newtonian fluids [4] the uncertainty in the governing equations rises. Because both gravity and surface tension act as wave restoring forces, there are two limiting regimes: those of the gravity waves and those of the capillary waves. A number of patterns ranging from spatially coherent patterns to localized states were observed in different parameter ranges [5,6].

Considerable attention has been paid to the problem of pattern formation outside of equilibrium partly due to the generic features in many different fields [7]. One of these is that very often primary patterns emerge when the external energy input (the driving) exceeds the output (the dissipation) in the initial quiescent state. There is usually a control parameter f that characterizes the driving strength, such as the accelerating amplitude in Faraday waves. When f reaches a threshold value f_c, in many cases the system is excited at a particular wave number k_c (for example, categories I and II in Ref. [3]), and a range of wave numbers becomes linearly unstable when $f>f_c$.

If f is near f_c, very often an amplitude equation description is found to be useful. In such a picture the system is considered to be described by a particular wave number, with the amplitude varying slowly in time and space. The analog to phonon modes in a crystalline solid may have some truth. As an example, in Faraday waves near threshold, patterns with different symmetries were observed [5]. These patterns are understood by a description in which amplitude evolution equations of a number of plane waves all at k_c but in different directions are considered. Correct predictions of pattern selection, i.e., the correspondence between particular patterns and experimental parameters, then come from calculations of the interaction between these plane waves from the basic fluid equations of motion [8].

On the other hand, in this paper we would like to consider how the coupling between different wave numbers affects wave dynamics. This approach of nonlinear wave dynamics of course will only be valid in the weakly nonlinear regime, where the distinction between different plane wave modes is still meaningful. Since the primary instability is previously found to have a transition from supercritical to subcritical bifurcations at a wave number a little larger than k_c [9], it is very likely that the dynamics of nonlinear waves that involve multiple wave numbers around k_c would exhibit interesting behavior.

Although the coupling in the pattern selection problems was obtained by a systematic analytical expansion of the Navier-Stokes equation [8] of the small parameter $\epsilon \equiv (f - f_c)/f_c$, the analysis was actually too complicated to be done by hand and symbolic computations were used. In principle a similar procedure can be followed to calculate coupling between different wave numbers, and with this information some aspects of the wave dynamics can be predicted. However, we foresee that this process will be even more complicated than that in the previous case. So for now we use numerical simulations to observe wave dynamics and infer its relationship with wave mode coupling.

Numerical simulations have given results that agree with the nonlinear expansion [9] with regard to bifurcations, and also showed good agreement with a recent experiment that carefully measured the saturated wave amplitudes [10]. In simulations there is more flexibility for control of the wave number and the initial conditions. This is somewhat difficult to achieve experimentally. We are currently limited to simulations in two dimensions, one vertical direction inside the fluid plus one of the horizontal directions. Full three-dimensional simulations are beyond our computational capacity.

In the simulations we first study the nonlinear saturated wave amplitudes (denoted by a *) for an individual wave number $A^*(k)$. Even though the linear instability is symmetric around k_c (at least, near k_c), the subcritical bifurcations at larger k make $A^*(k)$ very asymmetric between $k>k_c$ and $k<k_c$. Second, we observe wave dynamics with multiple

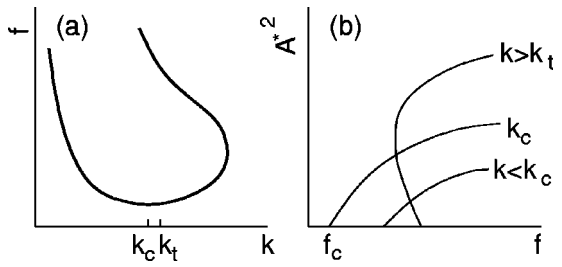

FIG. 1. (a) Linear instability diagram in the driving amplitude f and wave number k plane. The encircled region is the parameter range in which the wave will be excited subharmonically. (b) Illustrations of the dependence of nonlinear saturated wave amplitudes on driving at different wave numbers.

wave modes. It will be shown that the dynamics have good correlation with $A^*(k)$. Near the gravity wave regime, we also found interesting temporal modulations in the wave dynamics with a time scale much longer than the wave period. This phenomenon has some resemblance to the wave modulations observed in water channels [11], although complete theoretical understanding is still lacking.

Recently it was demonstrated [10] that nice regular rolls can be obtained in all parameter ranges in a rectangular cell with a length to width ratio exceeding, say, about five. The waves align perfectly perpendicular to the long side, even though the underlining wavelength is still much smaller than the cell width. The width could be, for example, ten times larger than the wavelength, thus ensuring negligible boundary effects. With this setup the results of our two-dimensional simulations can be directly compared.

This paper is organized as follows: in Sec. II we briefly discuss the nature of linear instability, bifurcation, a description of the amplitude equation, and the numerical methods. Results and discussion are presented in Sec. III, and a conclusion is given in Sec. IV.

II. INSTABILITY, BIFURCATION, AND NUMERICAL METHODS

For a liquid layer with a free surface subjected to sinusoidal vertical vibration, linear analysis [12–14] has shown that surface waves grow when the vibration amplitude f exceeds a frequency-dependent threshold value. A typical linear instability diagram is shown in Fig. 1(a) in the driving amplitude–wave number plane. The solid line encircles the region in which waves are excited at half the driving frequency. Typically the lowest driving threshold is at these subharmonic excitations, although there are some parameter ranges in which we expect harmonic responses [14,15].

The critical wave number k_c is indicated in Fig. 1(a) and its relationship with the driving frequency ω constitutes the dispersion relation. In the limit of zero viscous damping and an infinite fluid depth, it is $\omega_0^2 = g_r k_c + \sigma k_c^3/\rho$, with $\omega_0 = \omega/2$, g_r the gravitational acceleration, σ the surface tension, and ρ the fluid density.

The wave number k_c is expected to be excited when f is increased gradually across f_c. This instability is a supercritical bifurcation at k_c [9]. Thus near threshold, a description of

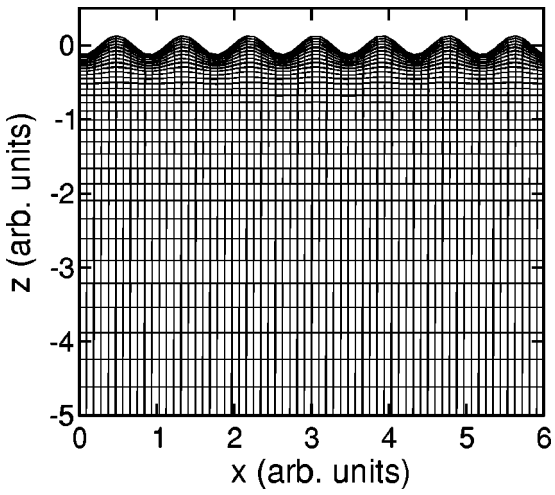

FIG. 2. Example of numerical grid systems in the simulations. Fewer grids than those used in the simulations are shown for clarity.

the amplitude equation for wave amplitude A is

$$\frac{\partial A}{\partial t} = \epsilon A - g A^3.$$

Here $\epsilon \propto f - f_c$ measures the distance above the threshold and g, the nonlinear coefficient is positive for supercritical bifurcation. There is no square term due to the $A \leftrightarrow -A$ symmetry. The nonlinear saturated wave amplitude A^* scales as $\sqrt{f-f_c}$, as depicted in Fig. 1(b) ($k=k_c$). When k is increased, it was found [9] that the bifurcation becomes subcritical above a particular k, which can be called the bicritical wave number k_t. The third order coefficient g becomes negative and a fifth order term is required to saturate the wave amplitude. Usually k_t is very close to k_c, not more than a few percent different most of the time. The saturated amplitudes A^* at $k>k_c$ and $k<k_c$ are also illustrated in Fig. 1(b).

Numerical simulations of wave dynamics are done for the incompressible Navier-Stokes equation,

$$\frac{\partial \mathbf{v}}{\partial t} + (\mathbf{v}\cdot\nabla)\mathbf{v} = -\frac{1}{\rho}\nabla p + \frac{\nu}{\rho}\nabla^2 \mathbf{v} - G(t)\hat{\mathbf{z}}. \tag{1}$$

Here $\mathbf{v}$ is the flow field, p the pressure, and ν the viscosity. This equation is written within a comoving framework (moving with the vertical vibration), such that the effective gravity term $G(t) = g_r + f\cos\omega t$.

A two-dimensional system with a free upper surface, a flat rigid bottom, and periodic boundary conditions in the horizontal direction is considered. Large fluid depth is used to approach the infinite depth limit. The space is discretized by a boundary conforming grid system, illustrated in Fig. 2, which is obtained by solving the Poisson equations,

$$\nabla^2 \xi(x,z) = P(x,z), \quad \nabla^2 \zeta(x,z) = Q(x,z).$$

Here (x,z) is the physical coordinate and (ξ,ζ) is the Cartesian coordinate in a computational rectangular domain [16]. The functions $P(x,z)$ and $Q(x,z)$ control the mapping be-

tween (x,z) and (ξ,ζ). Since the velocity is most significant near the free surface and decays into the fluid, we use $P(x,z)=0$ and $Q(x,z)=a\exp(-b|z-z_0|)$ (with a and b some suitable constants and z_0 the position of the flat surface) to obtain a grid system with denser grid lines near the free surface.

At each time-marching step, first the free surface is advanced according to the surface velocity, and then a new grid system is calculated under the new surface. The velocity at the interior points of the new grid is calculated from the Navier–Stokes equation. The pressure is determined by solving a pressure Poisson equation, which is obtained by taking $\nabla\cdot$ of Eq. (1), and eliminating the time derivative term with the incompressibility condition $\nabla\cdot\mathbf{v}=0$ [17]. On the free surface, the pressure and the horizontal and vertical components of velocity are determined by a combination of the normal stress boundary condition that involves the surface tension σ, the tangential stress condition, and the incompressibility condition. On the flat bottom the standard no-slip condition is used.

The time-marching scheme used is semi-implicit, such that the time evolution $\partial_t u=F$ for a particular variable u is computed by

$$u(t_{n+1})-u(t_n)=\frac{\Delta t}{2}[F(t_{n+1})+F(t_n)].$$

Over time, error accumulation if left unchecked will gradually produce deviation from the incompressibility condition $\nabla\cdot\mathbf{v}=0$. Thus at each step a correction $\delta\mathbf{v}$ is added to $\mathbf{v}$ to maintain $\nabla\cdot\mathbf{v}=0$. This correction is computed by

$$\delta\mathbf{v}=-\nabla B, \quad \text{with} \quad \nabla^2 B=\nabla\cdot\mathbf{v}.$$

Finally all the Poisson equations are solved by the successive-overrelaxation (SOR) method.

III. RESULTS AND DISCUSSIONS

In Faraday waves, physical parameters are usually made dimensionless by using $1/\omega_0$ as the time scale and $1/k_0$, with k_0 defined by the inviscid dispersion relation $\omega_0^2=g_r k_0+\sigma k_0^3/\rho$, as the length scale. Since we consider only infinite-depth fluids, the system is characterized by two dimensionless parameters defined as $\Sigma=\sigma k_0^3/\rho\omega_0^2$ and $\gamma=2\nu k_0^2/\omega_0$. With a range of $0\leqslant\Sigma\leqslant 1$, Σ is the measure of capillarity: $\Sigma=0$ being the pure gravity waves and $\Sigma=1$ the pure capillary waves. The parameter γ reflects the damping level.

First we consider the nonlinear saturated wave amplitudes at different wave numbers: $A^*(k)$. The wave numbers are set in simulations by using different system sizes. It is found that the dependence of $A^*(k)$ on the driving amplitude f can be roughly classified into three regions in the $\Sigma-\gamma$ parameter plane by the relative amplitude among $A^*(k>k_c)$, $A^*(k_c)$, and $A^*(k<k_c)$. The locations of these regions are indicated in Fig. 3a.

Typical examples of $A^*(k)$ as functions of f in the different regions are shown in Figs. 3(b)–3(d). An example of region I is shown in Fig. 3(b) and it occupies the largest

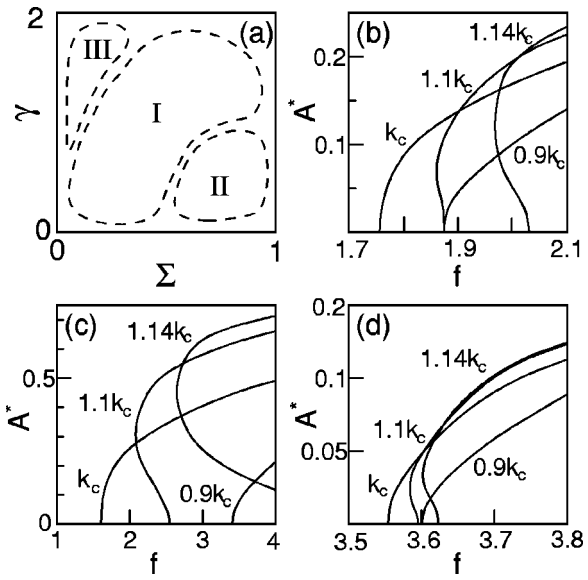

FIG. 3. (a) Locations of the three regions in the $\Sigma-\gamma$ plane. (b) Example in region I with $\Sigma=0.47$ and $\gamma=0.30$. (c) Example in the region II with $\Sigma=0.83$ and $\gamma=0.08$. (d) Example in region III with $\Sigma=0$ and $\gamma=1.97$. All units in (b)–(d) are arbitrary.

portion of parameter space. The initial $\sqrt{f-f_c}$ scaling of A^* and the subcritical bifurcation at larger k are clearly seen. At higher f, $A^*(k>k_c)$ is larger than $A^*(k_c)$, and at the same time $A^*(k<k_c)$ is generally smaller. The reason for this difference is naturally attributed to the subcritical bifurcations.

Region II is located near the capillary wave regime ($\Sigma\rightarrow 1$) at small damping. The $A^*(k)$ dependences seen in Fig. 3(c) have a similar global picture as those in Fig. 3(b) but with one significant difference. That is, the ratio between $A^*(k>k_c)$ [e.g., $1.1k_c$ in Fig. 3(b)] and $A^*(k_c)$ is significant larger than in the previous case. These larger amplitudes at $k>k_c$ will later be shown to contribute to the stability of $A(k>k_c)$ in dynamics involving multiple wave numbers.

It should also be stressed that, although we have indicated three distinct regions in Fig 3(a), the dashed lines are not meant to be viewed as sharp boundaries. Rather, the dependence of the saturated amplitude changes gradually with the parameters and the dashed lines in Fig. 3(a) are only guides to general locations.

For region III near $\Sigma=0$, a typical example is given in Fig. 3(d). The most significant aspect is that now the differences among $A^*(k>k_c)$, $A^*(k_c)$, and $A^*(k<k_c)$ are smaller compared to in the previous two cases. In the following we will show that in this region the waves exhibit very interesting modulated dynamical behavior.

Now we move on and discuss different dynamics that appear in these three regions. For a particular set of parameters, the size of the system is chosen to be $N\lambda_c$ ($\lambda_c=2\pi/k_c$ and N in the range of 5–14), such that the allowed wave numbers are k_c, $k_c\pm\Delta k$, $k_c\pm 2\Delta k$, ..., with $\Delta k\equiv k_c/N$. According to Fig. 1(a), above threshold we can have multiple wave numbers all being linearly unstable. In typical pattern formation systems, the resulting wave number is determined by some selection mechanisms, for example, rigid side wall, focus singularity in concentric rolls, dislocations,

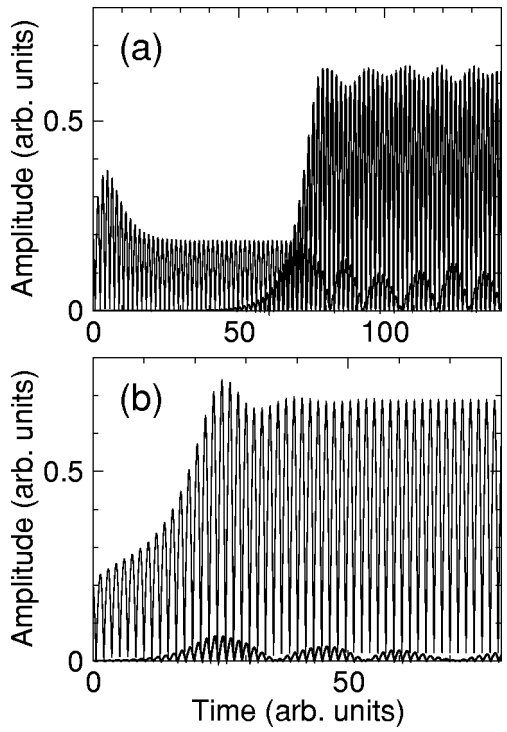

FIG. 4. (a) Time evolutions with the initial condition of a large amplitude for $k<k_c$ in region I. The thin line is for $\frac{6}{7}k_c$ and the thick line for k_c. (b) Time evolutions with the initial condition of a large amplitude for $k>k_c$ in region II. The thin line is for $\frac{8}{7}k_c$ and the thick line for k_c.

etc. [3]. Here, however, we like to see the competition among different wave numbers without any of these external influences.

The first test is whether a wave nonlinearly saturated at k_c would shift toward higher or lower k, as f is increased. In regions I and II, it is observed that mode k_c maintains its amplitude with an increase of f, such that Fourier components other than k_c all decay. Of course this may be due to the restriction of discrete wave numbers resulting from the finiteness of the system.

On the other hand, when mode $k_c-\Delta k$ is maintained at its saturated amplitude [with $f>f_c(k_c-\Delta k)$], we find that the mode k_c grows from a very small amplitude. A typical time evolution is shown in Fig. 4(a). The $A_{k_c-\Delta k}$ component (the thin line) reaches a steady amplitude about 0.2 after an initial transient period, but the component A_{k_c} depicted by the thick line grows under $A^*_{k_c-\Delta k}$. Eventually wave number k_c dominates even when there is a range of unstable modes.

It should be noted that the process of $A_{k_c-\Delta k}$ decaying and of A_{k_c} reaching steady amplitude exhibits modulated behavior at more or less regular intervals. A similar tendency also occurrs in other situations and parameters, although we have not yet understood their possible significance.

We can try to understand the results from an amplitude equation picture. In such a picture the time evolution is described by

$$\partial_t A_{k_c}=\epsilon_{k_c}A_{k_c}-g_{k_c}A_{k_c}^3-g_{k,k_c}A_k^2A_{k_c},$$

$$\partial_t A_k=\epsilon_k A_k-g_k A_k^3-g_{k_c,k}A_{k_c}^2A_k,$$

with $k\neq k_c$. Here ϵ_k and g_k are the linear growth rate and individual-mode nonlinear coefficient, respectively. Couplings $g_{k_c,k}$ and g_{k,k_c} describe the interaction strengths. The results in Fig. 4(a) imply that for $k=k_c-\Delta k$, $\epsilon_{k_c}-g_{k,k_c}A_k^{*2}>0$, and $\epsilon_k-g_{k_c,k}A_{k_c}^{*2}<0$. Without any knowledge of the values of g_{k,k_c} and $g_{k_c,k}$, we consider this to be plausible since $\epsilon_{k_c}>\epsilon_k$ and $A^*_{k_c}>A^*_k$.

In the opposite case of $k=k_c+\Delta k$, the results are similar to those of $k_c-\Delta k$ in region I. However, for the parameters in region II, we obtain a different result: the saturated amplitude $A^*_{k_c+\Delta k}$ is stable as a steady state, contrary to in the case of $k_c-\Delta k$. A typical time evolution is shown in Fig. 4(b) in which the component of $k_c+\Delta k$ reaches a steady amplitude while the k_c mode decays to zero.

The stability of $k_c+\Delta k$ in region II we believe is due to its large amplitude [cf. Fig. 3(c)]. As indicated previously, the ratio $A^*(k_c+\Delta k)/A^*(k_c)$ is larger in region II than in region I. If we argue that the coupling constant g_{k,k_c} does not vary too much at different k, the large $A^*(k_c+\Delta k)$ could yield a negative growth rate for A_{k_c}, which is given by $\epsilon_{k_c}-g_{k,k_c}A_k^{*2}$.

Region III is located near the gravity wave regime, which usually can be achieved by driving the system at lower frequencies. For example, with water as the working fluid, we have $\Sigma\sim 0.07$ at a driving frequency of 10 Hz. For $\Sigma=0$ and $\gamma=1.97$, with a system size of $7\lambda_c$, just above the threshold, the wave at k_c grows to its saturated value when all other modes decay. This is true even when the driving has exceeded $f(k_c\pm\Delta k)$.

When the driving is further increased, we find that the modes at wave numbers $k\neq k_c$ start to grow under $A^*_{k_c}$. This is demonstrated in the upper graph of Fig. 5. For clarity only amplitudes of k_c and $k_c+\Delta k$ are shown in the upper graph. $k_c+\Delta k$ always has the largest amplitude of all the non-k_c modes.

These non-k_c modes gradually grow to appreciable amplitudes. At some point A_{k_c} can no longer maintain its saturated value and quickly drops to a very small value, as though it is suppressed by the growing non-k_c modes. Here an interesting thing happens. Mode $k_c+\Delta k$ (also for other k) does not seize the opportunity of a small A_{k_c} to reach and maintain its full nonlinear saturated value, although f is indeed larger than $f_c(k_c+\Delta k)$. Instead the non-k_c modes follow the decline of k_c. Now it seems that the suppressing effects on A_{k_c} are gone with diminishing of the non-k_c modes, and A_{k_c} quickly reverts back to its original value. With A_{k_c} back to its full value and $A_{k\neq k_c}$ small, the scenario starts all over again with $A_{k\neq k_c}$ gradually growing.

In the upper graph of Fig. 5, the amplitudes of wave number k_c (the thick line) and $k_c+\Delta k$ (the thin line) display the periodic drop of A_{k_c} accompanied by the growth of $A_{k_c+\Delta k}$, which could continue indefinitely. In the lower graph an en-

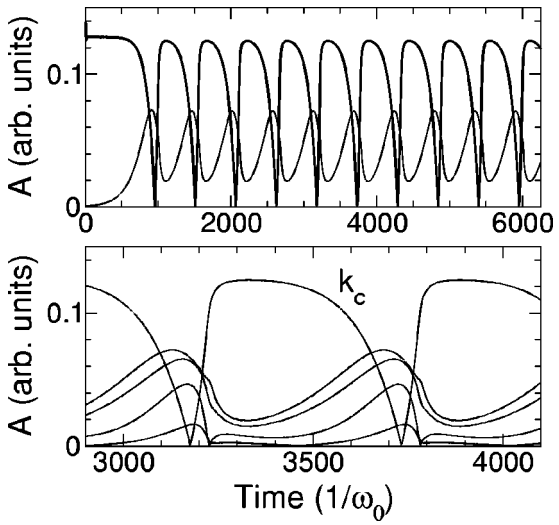

FIG. 5. Time evolutions of different components that exhibit punctuated behavior. For clarity, only wave numbers k_c (the thick line) and $k_c+\Delta k$ (the thin line) are shown in the upper graph. In the expanded plot shown in the lower graph, besides k_c, the wave numbers are $k_c+\Delta k$, $k_c-\Delta k$, $k_c+2\Delta k$, and $k_c-2\Delta k$ in descending order of the amplitudes.

larged view of a particular period is shown and the growth of amplitudes $A(k\neq k_c)$ are clearly seen. Among these wave numbers, $A(k_c+\Delta k)$ is the largest and $A(k)$ decreases as k away from k_c. It should also be stressed that the ratios of these amplitudes remain the same with different initial conditions after one or two transient periods. This indicates intrinsic dynamical behavior and that properties such as the elapsed time ΔT between two disruptions of $A(k_c)$ are intrinsic. Note that the lines in Fig. 5 depict the envelopes of the real wave amplitudes, which oscillate subharmonically with the driving frequency. (There are roughly 90 wave oscillations inside each periodic modulation for the case in Fig. 5.)

It is naturally expected that the elapsed time ΔT is determined mainly by the growth rates of $A(k\neq k_c)$. These growth rates should depend strongly on external driving. Indeed, it is seen in Fig. 6(a) that elapse time ΔT is shortened with an increase of f.

So what happens when A_{k_c} drops? A wave profile is plotted in Fig. 7 near the A_{k_c} disruption. The decrease in A_{k_c},

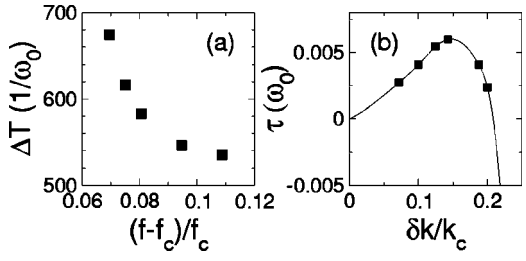

FIG. 6. (a) Elapsed time (in units of $1/\omega_0$) between two disruptions of $A(k_c)$ as a function of driving amplitude f. (b) Growth rates (in units of ω_0) of wave components under $A^*(k_c)$. There is an additional point at $(0.25,-0.041)$ not shown and the line is just a guide to the eye.

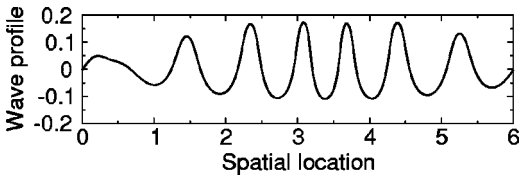

FIG. 7. Surface wave profile around the time of $A(k_c)$ disruption for $\Sigma=0$ and $\gamma=1.97$. The units are arbitrary.

accompanied by the significant amplitudes of both $A_{k_c\pm\Delta k}$, results in a beating envelope which has periodicity of $2\pi/\Delta k$, i.e., the size of the system. Conventionally we may tend to describe such a state by modulation of the wave amplitude: $A(K)\sin k_c x$, with K the modulation wave number. In the standard theoretical treatment this form is substituted into the equations of motion to derive a dynamical equation for $A(K,t)$. However, we believe that this approach is not usable here, since it is difficult to obtain the behavior observed even if we want to artificially construct a dynamical equation for $A(K,t)$.

The growth of $A_{k\neq k_c}$ under $A^*_{k_c}$ is a result of two contributions. The first is ϵ_k, the distance of f over the critical threshold $f_c(k)$. The second comes from the interaction between A_{k_c} and A_k. Since the simulations take place in a finite system, the wave numbers closest to k_c allowed are $k_c\pm\Delta k$. Thus the beating from k_c and $k_c\pm\Delta k$ necessarily gives an envelope at wave number Δk as seen in Fig. 7. Of course, if the maximum growth and the largest amplitude happen at $k_c\pm 2\Delta k$, we could have a shorter-period beating envelope. This however is unfavorable according to ϵ_k which becomes small (even negative) when k is away from k_c.

On the other hand, near k_c, ϵ_k would increase. If this is also true for the resulting net growth rate, the beating envelope will have periodicity that increases with the size of the system. But this is not the case observed. We measure the small amplitude growth rate τ for A_k at different $\delta k=k-k_c$ under $A^*_{k_c}$. The results are plotted in Fig. 6(b). The growth rate τ is only positive in a range of δk and, more significantly, has a maximum at a particular δk_m. This ensures that there is a definite period of the beating envelope and that the slow modulating time scale is independent of the system's size. The reason for a maximum may be understood from the fact that, as $\delta k\to 0$, we necessarily need $\tau\to 0$, since wave number k_c is already at its full value. Furthermore, the second contribution to τ is due to $g_{k_c,k}$, whose values we might take by inference from g_k (the cube coefficient for A_k). Since g_k changes sign at a particular k_t (the subcriticality) such that at $k>k_t$, g_k promotes the growth of A_k and the opposite effect at $k<k_t$.

As we have shown in Fig. 3(d), there is the tendency that in the current case all three wave modes, $A^*(k_c)$ and $A^*(k_c\pm\Delta k)$, have comparable single-mode saturated amplitudes. This might be a hint as to the origin of the modulating dynamics. Here we would like to emphasis again that all components other than A_{k_c} grow at fixed ratios, regardless of the initial conditions. Even the system started with the saturated amplitude $A^*_{k_c+\Delta k}$ and a very small A_{k_c}, A_{k_c} will gradu-

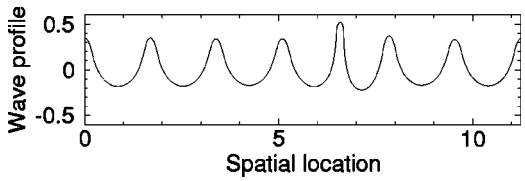

FIG. 8. Surface wave profile around the time of $A(k_c)$ disruption at a small damping parameter $\gamma=0.16$ ($\Sigma=0$). The units are arbitrary.

ally grow. Eventually we go back to what is seen in Fig. 5. It differs from what was shown for region II where both A_{k_c} and $A_{k_c+\Delta k}$ can be the final steady amplitudes, depending on the initial conditions.

If we set the system parameters at $\gamma=0.16$ (again with $\Sigma=0$), a similar picture is again seen. However this time at the disruption of A_{k_c}, the wave exhibits a different profile, which is shown in Fig. 8. One of the waves becomes a peaked, solitary-like structure. Which one transforms depends on the arbitrarily chosen initial phase of $A_{k\neq k_c}$. Unfortunately, the solitary structure causes difficulty in the numerical simulations and the simulations cannot be run further after a certain point. Nevertheless all the results up to this point are consistent with the picture described above for larger γ.

IV. CONCLUSION

In Faraday waves with infinite fluid depth, we have found three different dependences of nonlinear saturated wave amplitudes on the driving strengths, classified by the relative amplitudes among different wave numbers. Distinct wave dynamics are then observed in these different dependences, and the dynamics are closely related to the single-mode saturated wave amplitudes. In one regime we find that both the critical and higher wave numbers can be stable as steady states, depending on the initial conditions. In the other regime we see the appearance of a new slow time scale that is much longer than the original wave period. Finally, we believe that this interesting slow modulated dynamics near the gravity wave regime should be looked for in experiments.

ACKNOWLEDGMENT

This work was supported by the National Science Council of Taiwan.

[1] M. Faraday, Philos. Trans. R. Soc. London **121**, 319 (1831).
[2] H. W. Müller, R. Friedrich, and D. Papathanassiou, *Evolution of Spontaneous Structures in Dissipative Continuous Systems*, edited by F. Busse and S. C. Müller, Lecture Notes in Physics, Vol. 55 Müller, (Springer, New York, 1998).
[3] For a review, see, M.C. Cross and P.C. Hohenberg, Rev. Mod. Phys. **65**, 851 (1993).
[4] H.W. Müller, Phys. Rev. E **58**, 6199 (1998); F. Raynal, S. Kumar, and S. Fauve, Eur. Phys. J. B **9**, 175 (1999); O. Lioubashevski, Y. Hamiel, A. Agnon, Z. Reches, and J. Fineberg, Phys. Rev. Lett. **83**, 3190 (1999); C. Wagner, H.W. Müller, and K. Knorr, *ibid.* **83**, 308 (1999); H. Arbell and J. Fineberg, *ibid.* **84**, 654 (2000); H.-J. Pi *et al.*, *ibid.* **84**, 5316 (2000).
[5] B. Christiansen, P. Alstrøm, and M.T. Levinsen, Phys. Rev. Lett. **68**, 2157 (1992); W.S. Edwards and S. Fauve, Phys. Rev. E **47**, R788 (1993); J. Fluid Mech. **278**, 123 (1994); M. Torres, G. Pastor, I. Jiménez, and F. Montero de Espinosa, Chaos, Solitons Fractals **5**, 2089 (1995); T. Besson, W.S. Edwards, and L.S. Tuckerman, Phys. Rev. E **54**, 507 (1996); A. Kudrolli and J.P. Gollub, Physica D **97**, 133 (1996); D. Binks and W. van de Water, Phys. Rev. Lett. **78**, 4043 (1997); D. Binks, M.-T. Westra, and W. van de Water, *ibid.* **79**, 5010 (1997).
[6] O. Lioubashevski, H. Arbell, and J. Fineberg, Phys. Rev. Lett. **76**, 3959 (1996).
[7] M. I. Rabinovich, A. B. Ezersky, and P. D. Weidman, *The Dynamics of Patterns* (World Scientific, Singapore, 2000).
[8] P. Chen and J. Viñals, Phys. Rev. Lett. **79**, 2670 (1997); Phys. Rev. E **60**, 559 (1999).
[9] P. Chen and K.-A. Wu, Phys. Rev. Lett. **85**, 3813 (2000).
[10] A. Wernet, C. Wagner, D. Papathanassiou, H.W. Müller, and K. Knorr, Phys. Rev. E **63**, 36305 (2001).
[11] See, e.g., B.M. Lake, H.C. Yuen, H. Rungaldier, and W.E. Ferguson, J. Fluid Mech. **83**, 49 (1977); W. Melville, *ibid.* **128**, 489 (1983); L. Jiang, C.-L. Ting, M. Perlin, and W.W. Schultz, *ibid.* **329**, 275 (1996); I. Shugan and K. Voliak, *ibid.* **368**, 321 (1998); M.P. Tulin and T. Waseda, *ibid.* **378**, 197 (1999).
[12] T. Benjamin and F. Ursell, Proc. R. Soc. London, Ser. A **225**, 505 (1954).
[13] K. Kumar and L.S. Tuckerman, J. Fluid Mech. **279**, 49 (1994).
[14] K. Kumar, Proc. R. Soc. London, Ser. A **452**, 1113 (1996).
[15] H.W. Müller *et al.*, Phys. Rev. Lett. **78**, 2357 (1997).
[16] For further details, see, e.g., *Numerical Grid Generation*, edited by J. F. Thompson (North-Holland, Amsterdam, 1982).
[17] See, e.g., C. Pozrikidis, *Introduction to Theoretical and Computational Fluid Dynamics* (Oxford, New York, 1997).